

Planning and Operation Stochastic Optimization Model of Power Systems Considering the Flexibility Reformation

Xu H., Li H.

1. ICP Inst. of Computational Physics, ZHAW Zurich University of Applied Sciences, Switzerland
2. UiT - The Arctic University of Norway
3. Al Ghurair University, UAE
4. Oslo Metropolitan University, Norway

ABSTRACT

A finite volume based Eulerian-Lagrangian model has been created within OpenFOAM® in order to predict the behavior of particle clouds as well as particle deposition thicknesses on substrates under the influence of electrostatic effects. The model resolves close to electrode effects as well as phenomena within the entire deposition chamber. It considers fluid dynamic effects, particle inertia, gravity, electric- as well as mechanic particle-particle interaction, corona formation, dynamic particle charging mechanisms, and coupling of particle motion to Reynolds-Averaged Navier-Stokes (RANS) based flow simulations. Resulting deposition pattern predictions were experimentally validated. It is demonstrated qualitatively and quantitatively that the measured deposition thicknesses and patterns vary by; i) applied voltage, ii) airflow rate, pistol-substrate iii) distance and iv) angle. Furthermore, the software has been prepared such that it works on the cloud computing software KaleidoSim®, which enables the simultaneous browser-based running of hundreds of cases for large parameter studies.

1. INTRODUCTION

The prediction and understanding of deposition patterns in the context of electrostatic spraying applications has been a challenge for decades. Even highly automatized spray-deposition installations still lack the ability to adapt process parameters such as airflow rate, applied voltage, deposition particle injection intensity, as well as distance and angle between deposition pistol and substrate to varying substrate geometries. In consequence, yielding imperfect depositions and considerable local variations in deposition thickness. A first step towards creating a procedure to automatically define suitable deposition process parameters for any substrate geometry, is the validated modeling of such applications involving fluid and particles parameters.

Multiphysics models involving fluids and particles have evolved over the years predicting various engineering applications. For example, researchers have developed models for particle-laden flows [1, 2], electrochemical process [3, 4], viscosity and density measurements [5], wood gasification [6, 7], fluidized beds [8-13], pyrolysis reactions [14], particle deposition [15-18], filtration process [19, 20] and more.

The particular study is a finite volume based Eulerian-Lagrangian model, which has been created in OpenFOAM® in order to predict the behavior of particle clouds as well as particle deposition thicknesses on substrates under the influence of electrostatic effects. Having inherited its basic functionality from icoLagrangianFoam [21] within outdated OpenFOAM® 1.4.1 as well as from an extensive non-spherical Eulerian-Lagrangian model (see [19] and [20]), the solver has been evolved over five years. Now it has become an OpenFOAM® 5.0 compatible, fully parallelizable tool. Going far beyond the capabilities of icoLagrangianFoam, the software does not only include flow and spherical particle dynamics but also electrostatic effects, the ability to model ionized oxygen distribution in the context of the corona-formation of a high-voltage electrode, dynamic charging of deposition particles as well as detailed particle-substrate interaction effects.

The overall modeling concept aims to predict the behavior of any cloud of deposition particles by an efficient, yet statistically relevant representation using a limited number of individual Lagrangian particles, rather than choosing a two-phase or two-species approach. Thereby, the point of the simulation is to understand deposition thickness distributions on any substrate under varying deposition process conditions such as i) applied voltage, ii) applied airflow, iii) distance between deposition pistol and substrate, iv) angle between deposition pistol and substrate.

In one-to-one analogy to standard validation experiments, the CFD model geometry (see Fig.1) is: i) a box-representation of the flow chamber featuring inlet- and outlet-vents with ii) a metallic plate acting as electrically grounded substrate, iii) approximately one-third of the frame of a deposition pistol, containing iv) a fully resolved air-particle flow tube which leads towards v) a high-voltage electrode and past vi) a nozzle into the deposition chamber. The idea is that an airflow laden with polymeric particles is injected at the primary inlet inside the pistol. The flow is then pushed past the high voltage electrode (featuring up to 100kV), where ionized oxygen attaches to the surfaces of the borne particles, enabling the electric field to affect particle motion. Said electric field is formed between the electrode within the pistol-frame and the electrically grounded substrate. Influenced by i) gravity, ii) fluid dynamic forces, as well as iii) electric forces, the charged particles pass through the nozzle and are sprayed towards the substrate, where they impact and either stick or get blown off.

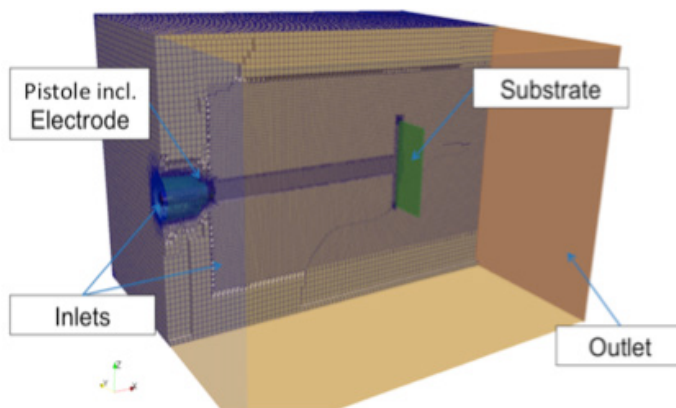


Fig.1: Basic model geometry including deposition pistol with a resolved electrode and particle airflow path (blue), substrate (green), primary inlet (left, inside the pistol, for particle laden flow), secondary inlet (left, outside pistol, for air) and outlet (right). Structured, hexahedral mesh with approx. four million cells.

Not only predictive quality of the simulation model but also applied software technology has been improved: i) update from OpenFOAM® 1.4.1 to 5.0, ii) introduction of full parallelization capability, as well as the enabling of iii) cloud-based design of experiments (DoE) and iv) high performance computing (HPC) capabilities, using KaleidoSim® [22] software.

Validation efforts have spanned thousands of deposition experiments, which lead to a vast number of qualitative and quantitative comparisons of deposition patterns and deposition thickness-measurements considering variations of the main process parameters: applied electrode voltages, airflow rates, distance pistol to a substrate, angle between pistol and substrate.

While sections 2.1 and 2.2 describe the evolution of the underlying physical model and of the applied simulation technology respectively, section 2.3 presents selected results from the validation-study, demonstrating a high level of agreement between predictions and experiments. The context of these results is consequently discussed in section 3.

2. METHODS AND RESULTS

The physical and technological capabilities of the particle deposition solver have been successively advanced over the years. In the following, the main stages of this evolution are briefly pointed out. Since the development has been closely accompanied by experimental validation, some selected comparisons to deposition thickness measurements are presented as well.

2.1. Evolution of the Physical OpenFOAM® Model

2.1.1. Particle dynamics and fluid-particle interaction: OpenFOAM® 1.4.1, icoLagrangianFoam

The initial Eulerian-Lagrangian solver version was a simple fork of the OpenFOAM® 1.4.1 based icoLagrangianFoam [21] code, extended by a more refined drag law. It encompassed particle dynamics as well as laminar flow calculation and gravity.

2.1.2. Electrostatic forces, buoyancy and particle-particle interaction: Including Poisson Equation and space charge density field

In a major adaption-phase the original solver version was extended to account for buoyancy, electrostatic forces and electric particle-particle interaction [1]. In order to achieve this, the stationary Maxwell equations were implemented, requiring the introduction of an electric potential field Ψ (Nm/C), an electric force field \vec{E} (N/C) as well as a space charge density field ρ_c (C/m³). On the basis of user selection, particle charges and/or ionized oxygen can affect the electrostatic field or be disregarded. In the latter case ρ_c features non-zero entries only at the electrode-boundary patch. The following governing equations show Faraday's Law of Induction (Eqn. 1), Gauss' Law concerning Electric Fields (Eqn. 2), the connection between Ψ and \vec{E} (Eqn.3) and the Poisson Equation (Eqn.4) relating Ψ and ρ_c . Finally, Eqn.5 shows the resulting particle momentum equation (Eqn.5), which is at the core of the implemented Lagrangian particle model [2].

$$\nabla \times \vec{E} = \vec{0} \quad \text{Eqn. 1}$$

$$\nabla \cdot \vec{E} = \rho_c / \epsilon_0 \quad \text{Eqn. 2}$$

$$\vec{E} = -\nabla \Psi \quad \text{Eqn. 3}$$

$$\Delta \Psi = -\rho_c / \epsilon_0 \quad \text{Eqn. 4}$$

$$\frac{\partial^2 \vec{x}_p}{\partial t^2} = \frac{\vec{v}_{rel}}{\tau_p} + \frac{\rho_p - \rho_F}{\rho_p} * \vec{g} + \frac{q_p D_p^2 \pi}{m_p} * \left(\vec{E} + \frac{D_p^2 \pi}{4 \epsilon_0} \nabla \rho_c \right) \quad \text{Eqn. 5}$$

In Eqn.5 \vec{x}_p (m) is the particle position, \vec{v}_{rel} (m/s) is relative particle flow velocity, ρ_p (kg/m³) and ρ_F (kg/m³) are particle and fluid density respectively, \vec{g} (N/kg) is the gravity vector, D_p (m), m_p (kg), and q_p (C/m²) are particle diameter, mass, and specific surface charge respectively, ϵ_0 (C/Vm) is the electric field constant, and τ_p (s) is the particle relaxation time.

The implementation of Eqn. 1 to Eqn. 4 enables an evaluation of the spatial electrostatic field between and within the vicinity of the electrode and the substrate. An exemplary field-line representation of the calculated field is depicted in Fig.2.

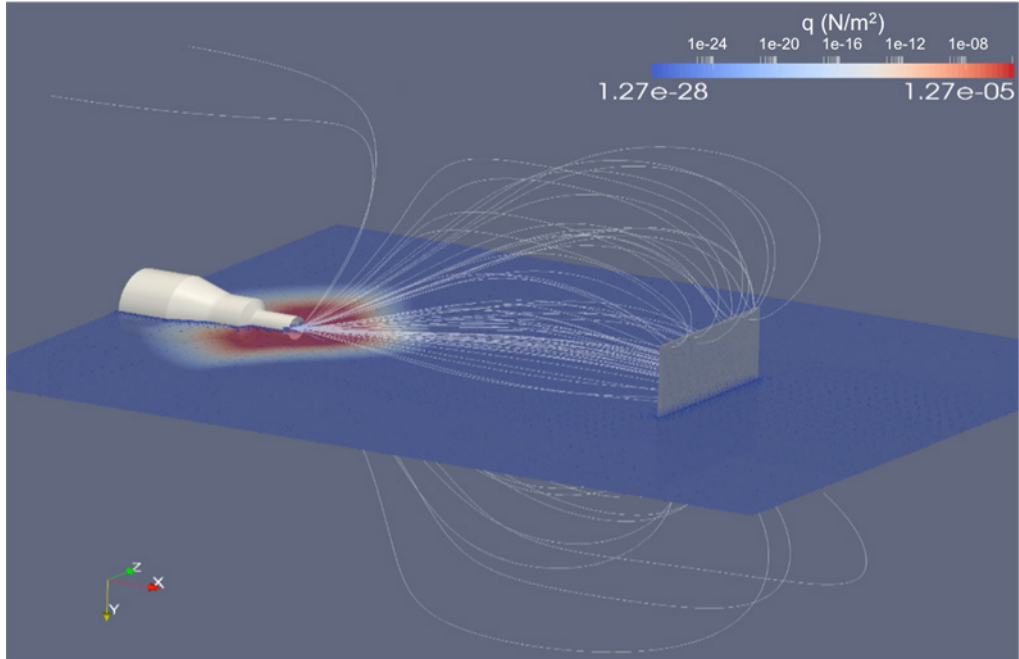


Fig.2: Field line representation of the electrostatic field between electrode and substrate. The color scheme represents space charge density q_c (C/m³) caused by ionized oxygen at the electrode.

2.1.3. Introducing the k-factor for particle flow interaction while using RANS turbulence modeling

An essential step towards achieving better applicability of the model was the implementation of a scheme to use efficient Reynolds-Averaged Navier-Stokes (RANS) based turbulence modeling while maintaining result accuracy in terms of particle distribution on the substrate [17]. The problem of RANS ensemble averaging of eddies and the consequential reduction of the particles' tendency to disperse was overcome by the introduction of the empirically adjusted k-factor γ_k (non-dimensional) (see Eqn.6 and Eqn.7). In Eqn.6 and Eqn.7 \vec{v}_f (m/s) is the fluid flow velocity, k (m^4/s^2) is the turbulent kinetic energy obtained by RANS (e.g., k- ϵ or SST k- ω) calculation and \vec{r} (non-dimensional) is a randomized unit vector.

$$\|\vec{v}'_f\| = \sqrt{\frac{2}{3}k} \quad \text{Eqn. 6}$$

$$\vec{v}_{f,mod} = \overline{\vec{v}_f} + \gamma_k \|\vec{v}'_f\| \vec{r} \quad \text{Eqn. 7}$$

Fig.3 shows a comparison between an experimentally derived deposition-pattern on the front side of a plate shaped metallic substrate and three simulated results where the k-factor was changed successively. The comparison shows that too low k-factors (here e.g., 0.5 and 1) lead to a qualitative underestimation of the particles' tendency to disperse across the substrate.

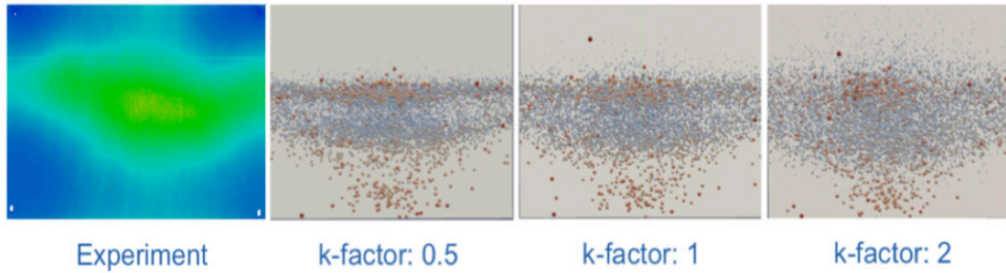


Fig.3: Deposition pattern on the front side of a plate shaped substrate. Derived from the experiment (left) and simulated based on k-factors 0.5, 1, and 2 respectively. Here k-factor = 2 shows the best qualitative deposition-pattern agreement with the experiment.

2.1.4. Corona modeling and dynamic particle charging

The model was furthermore extended to account for close to electrode effects. These effects encompass corona-formation phenomena [16] as well as particle charging dynamics. While the first is caused by oxygen ionization around the high voltage electrode [18], the latter occurs due to particles passing through the electrically charged corona. Because of varying local corona charge density q_c (C/m^3), varying charge transfer coefficients β_{cp} (m/s), and varying particle corona residence time t (s), each particle accumulates an individual charge portion, expressed as specific surface charge q_p (C/m^2). The introduction of a dynamic

particle charging model, described by Eqn. 8 and Eqn. 9, in combination with an empirical fitting procedure regarding the charge transfer coefficient (see Fig.4), leads to an increase of predictive quality of the whole model.

$$\frac{dq_p}{dt} = \beta_{cp} \left(1 - \frac{q_p(t)}{q_{p,\text{lim}}}\right) \left[q_c(\vec{X}, t) - \frac{6}{D_p} q_p(t)\right] \quad \text{Eqn. 8}$$

$$q_{p,\text{lim}} = D_p^2 \pi \varepsilon_0 |\vec{E}| \cdot \left(1 + 2 \cdot \frac{\varepsilon_{r,p}-1}{\varepsilon_{r,p}+1}\right) \quad \text{Eqn. 9}$$

In Eqn. 9 $\varepsilon_{r,p}$ (non-dimensional) is the relative electric permittivity of the particles, and $q_{p,\text{lim}}$ (C/m²) is the maximum achievable specific particle surface charge.

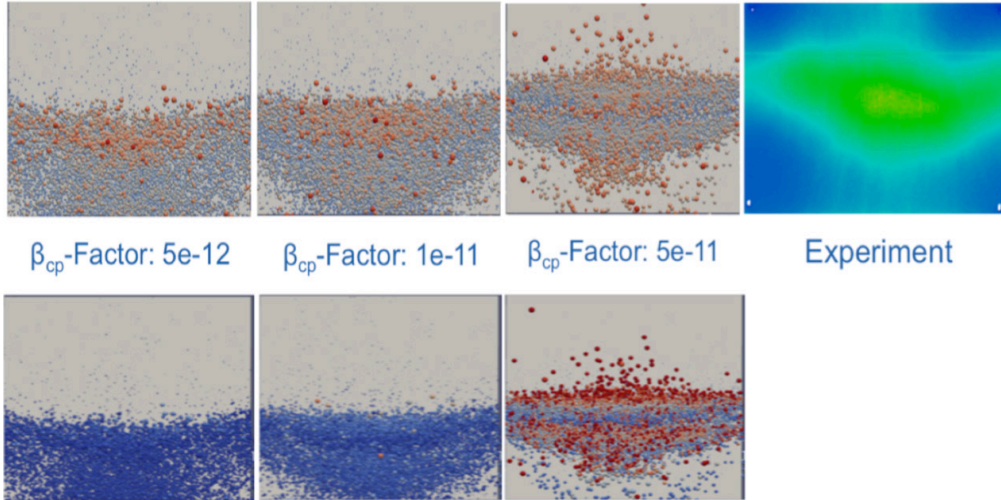


Fig.4: Qualitative example of empirical fitting of the charge transfer coefficient (β_{cp} -Factor) to an experimentally derived deposition pattern (top right). Coloring of simulated particles relates to particle diameter (top) from 1E-6m (blue) to 9.5E-5m (red) and variable particle surface charge (bottom) from 1.74E-8 C/m² (blue) to 1.0E-6 C/m² (red).

2.1.5. Effects of electrode and nozzle shape: Improving geometry and mesh

In addition to increasing the level of depth of the physical modeling, geometric model-detail was evolved as well. While previous model versions simply considered the deposition pistol outlet, evolved versions resolve the whole insides of individual pistols. Thus, it becomes possible to consider particle flow paths from the entry-tube, past the electrode towards the nozzle outlet. This improvement enables the consideration of design changes within the deposition pistol, concerning the electrode itself, as well as the nozzle outlet.

2.2. Technological Evolution of the OpenFOAM® Model

Aside from evolving the physical and geometric model, applied simulation technology has been improved as well.

2.2.1. From OpenFOAM® 1.4.1 to OpenFOAM® 5.0 and parallelization

Starting with an adaption of the icoLagrangianFoam solver under OpenFOAM® 1.4.1, instructions for updating the solver to OpenFOAM® 1.6 published in [21] were combined with own findings, to obtain a functional version for OpenFOAM® 5.0. Along with updating the code to OpenFOAM® 5.0, parallelization capabilities were introduced, such that considerable speed-up of calculation duration could be achieved, as shown in Fig.5.

2.2.2. KaleidoSim®

The worldwide accessibility of the software via internet-browser, as well as its capability to conduct dozens and even hundreds of simulation-runs simultaneously, were established by hosting the deposition solver on the novel cloud-computing platform KaleidoSim®. The Design of Experiment (DoE) module within KaleidoSim® enables the completion of extensive parameter studies in an extremely short time. The investigation of multi-parameter problems, which are quite common in industrial deposition applications, thus becomes much simpler and much faster.

2.2.3. Experimental methods and validation

Validation and model adaption efforts have been undertaken in order to prove and improve the predictive quality of simulated deposition patterns. A relatively simple, standardized experimental setup (see Fig. 6) was used in order to deposit particles on plate-shaped metallic substrates, dimensioned either according to A4 standard ('A4-plate') or 10cm x 10cm x 0.3cm ('small-plate'). Applying the Coatmaster 3D® [15, 23] deposition thickness detection and evaluation technology [15], approx. 5000 individual deposition measurements were taken and evaluated.

Based on these experiments, qualitative (for example, see Fig.7) and quantitative (see Fig.8 to Fig.11 for examples) correspondence between simulation-based deposition pattern predictions and reality was investigated. Representing a selected subspace of the total investigated system-parameter-space, the data depicted in Fig.8 to Fig.11 is based on 69 separate deposition experiments and 216 separate Coatmaster 3D® [15, 23] deposition thickness measurements. Within these experiments, a defined amount of particles were deposited on 'small-plates' at 23 different process parameter sets. Each experiment was repeated on three different plates, and each plate was measured three or six times, depending on whether only the front side or both front and back sides were evaluated. The 23 process parameter sets were chosen such that deposition thickness trends for a controlled variation of the essential process parameters could be investigated.

The particle deposition process parameters under investigation are: i) applied voltage, ii) applied airflow rate, iii) distance between pistol and substrate, and iv) angle between pistol and substrate.

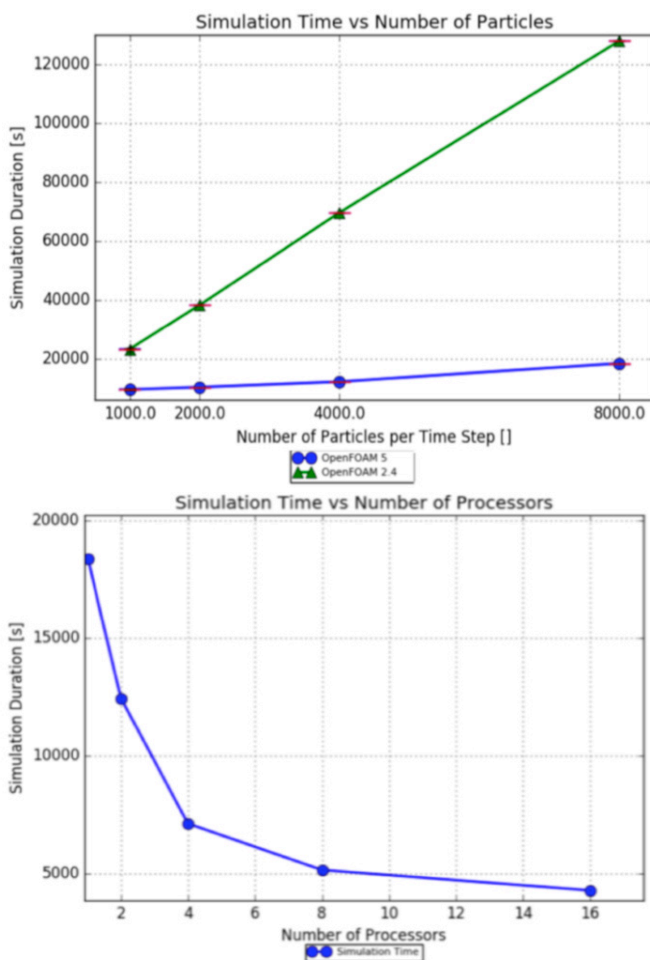


Fig.5: Left: Comparison of simulation duration of OpenFOAM® code versions 2.4 and 5.0 of single processor cases using 10,000 – 80,000 totally injected Lagrangian particles versus the number of injected particles per time step (using ten-time steps for injection). Right: Simulation duration of parallelized cases using 40,000 Lagrangian particles versus the number of applied processors. Both: Each simulation case is valid for pre-calculated, otherwise stationary electric- and fluid-fields within a standard- ‘small plate’ deposition setup, a four million cell geometry, spanning 0.6s of real-time deposition procedure as well as particle time steps of 4E-6s.

2.2.4. Experimental methods and validation

Validation and model adaption efforts have been undertaken in order to prove and improve the predictive quality of simulated deposition patterns. A relatively simple, standardized experimental setup (see Fig.6) was used in order to deposit particles on a plate-shaped metallic

substrates, dimensioned either according to A4 standard ('A4-plate') or 10cm x 10cm x 0.3cm ('small-plate'). Applying the Coatmaster 3D® [15, 23] deposition thickness detection and evaluation technology [15], approx. 5000 individual deposition measurements were taken and evaluated.

Based on these experiments, qualitative (for example, see Fig.7) and quantitative (see Fig.8 to Fig.11 for examples) correspondence between simulation-based deposition pattern predictions and reality was investigated. Representing a selected subspace of the total investigated system-parameter-space, the data depicted in Fig. 8 to Fig. 11 is based on 69 separate deposition experiments and 216 separate Coatmaster 3D® [15, 23] deposition thickness measurements. Within these experiments, 'small-plates' were deposited with a defined amount of particles at 23 different process parameter sets. Each experiment was repeated on three different plates, and each plate was measured three or six times, depending on whether only the front side or both front and back sides were evaluated. The 23 process parameter sets were chosen such that deposition thickness trends for a controlled variation of the essential deposition process parameters could be investigated.

The deposition process parameters under investigation are: i) applied voltage, ii) applied airflow rate, iii) distance between pistol and substrate, and iv) angle between pistol and substrate.

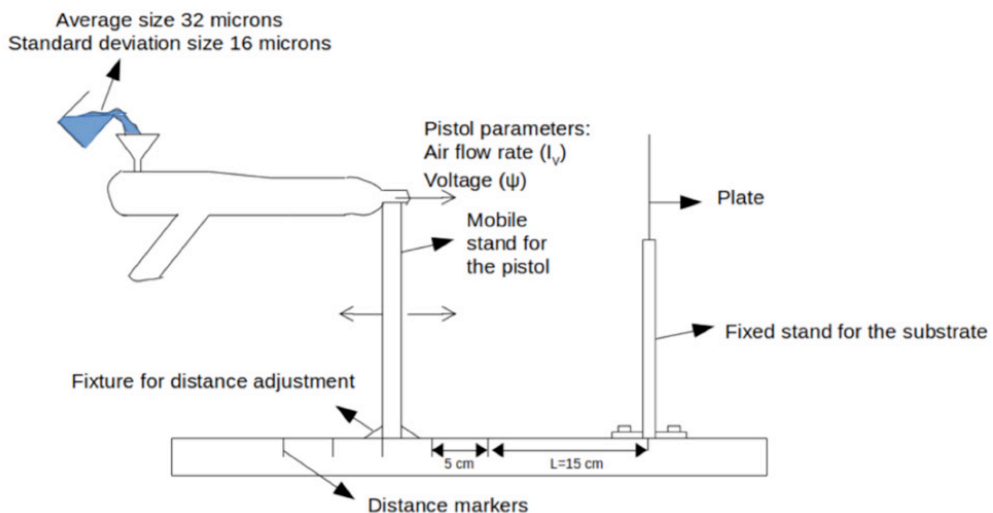


Fig.6: Standardized experimental deposition set-up.

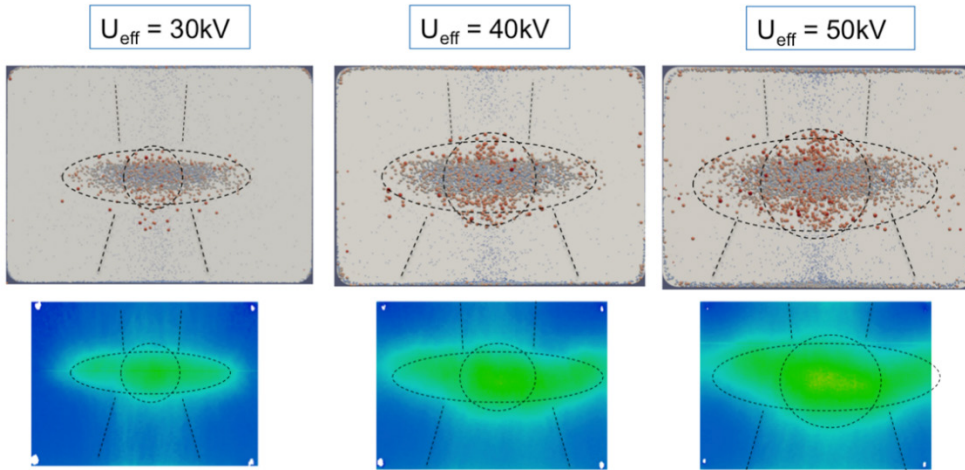


Fig.7: Example of qualitative correspondence of simulated (top) and measured (bottom) deposition patterns. Here the particles were deposited on the front side of an A4-plate substrate at a pistol to substrate distance of $D=20\text{cm}$ while applying an airflow rate $Q=3\text{m}^3/\text{h}$ and effective voltages U_{eff} of 30kV, 40kV and 50kV respectively. It can be seen that the main qualitative deposition pattern features, as well as trends of simulations and experiments, match well.

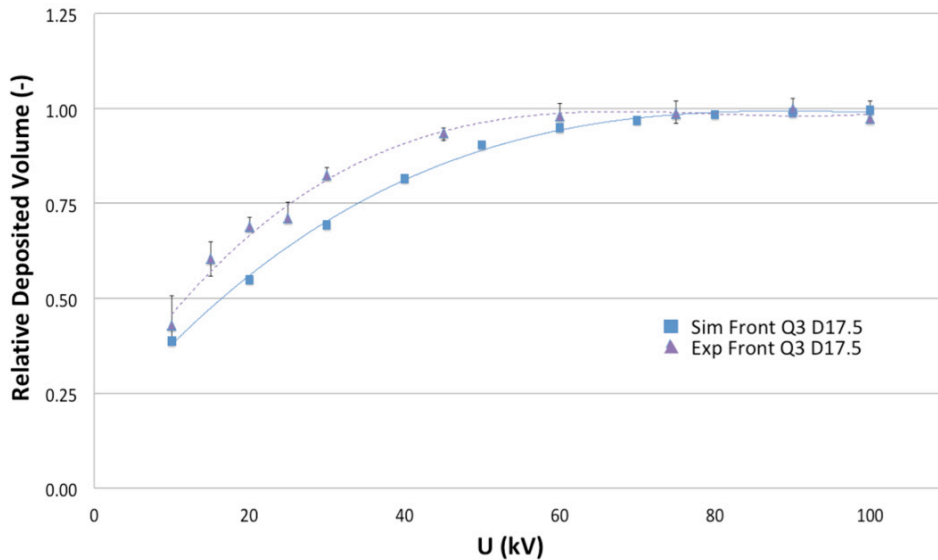


Fig.8: Quantitative comparison of relative deposited particle volume (normalized to maximum value) at the front side of 'small-plate' of simulations (blue, full) vs. processed experimental data (purple, dashed lines, including black bars for data variation limits) for varying applied voltages U (kV) at pistol to substrate distance of $D=17.5\text{cm}$ and an airflow rate $Q=3\text{m}^3/\text{h}$. Each depicted measurement data point is the median of three independent experiments and three consecutive deposition thickness measurements per experiment.

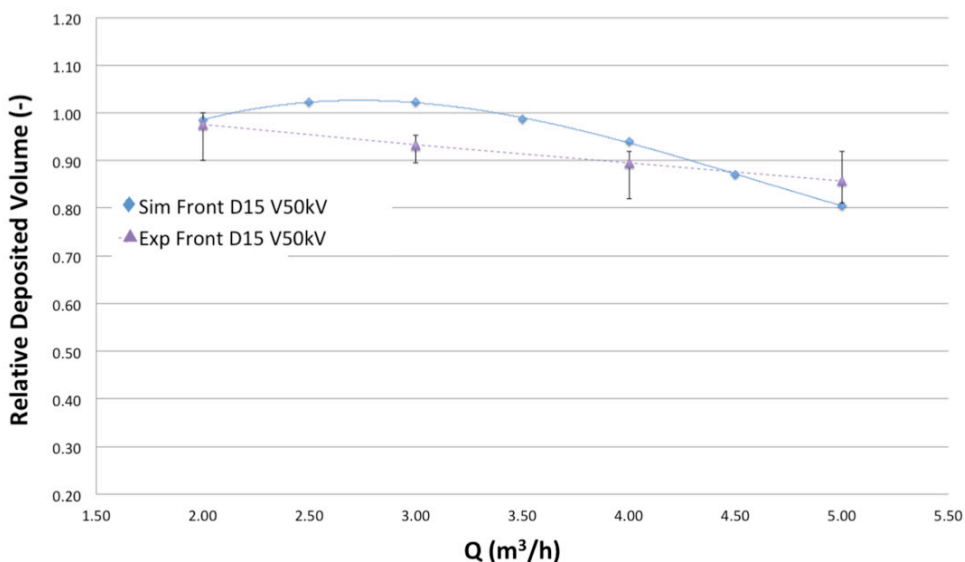


Fig.9: Quantitative comparison of relative deposited particle volume (normalized to value at $Q=2\text{m}^3/\text{h}$) at front-side of 'small-plate' of simulations (blue, full) vs. processed experimental data (purple, dashed lines, including black bars for data variation limits) for varying airflow rate Q at pistol to substrate distance of $D=15\text{cm}$ and effective voltage $U_{\text{eff}}=50\text{kV}$. Each depicted measurement data point is the median of three independent experiments and three consecutive deposition-thickness measurements per experiment.

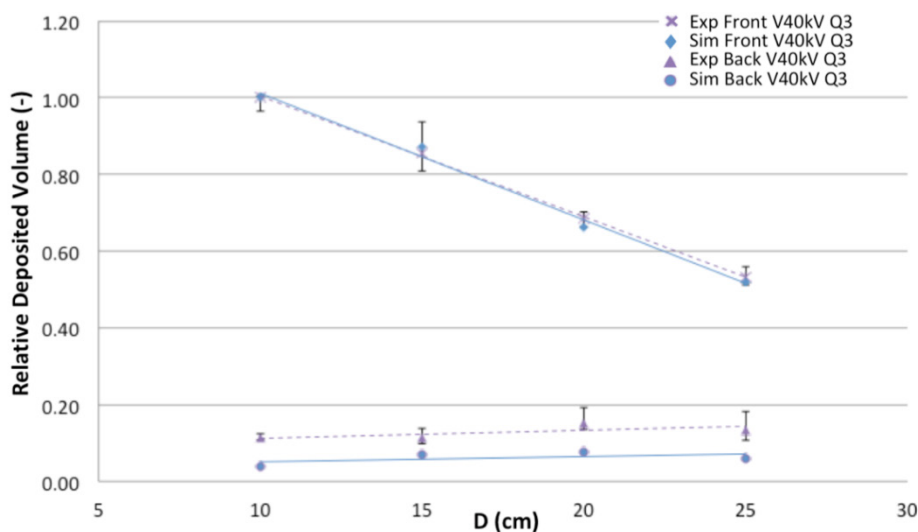


Fig.10: Quantitative comparison of relative deposited particle volume (normalized to maximum value) at front and back sides of 'small-plate' of simulations (blue, full) vs. processed experimental data (purple, dashed lines, including black bars for data variation limits) for varying pistol to substrate distance of D (varied) at $U_{\text{eff}}=40\text{kV}$ and $Q=3\text{m}^3/\text{h}$. Each depicted measurement-data-point is the median of three independent experiments and three consecutive thickness measurements per experiment.

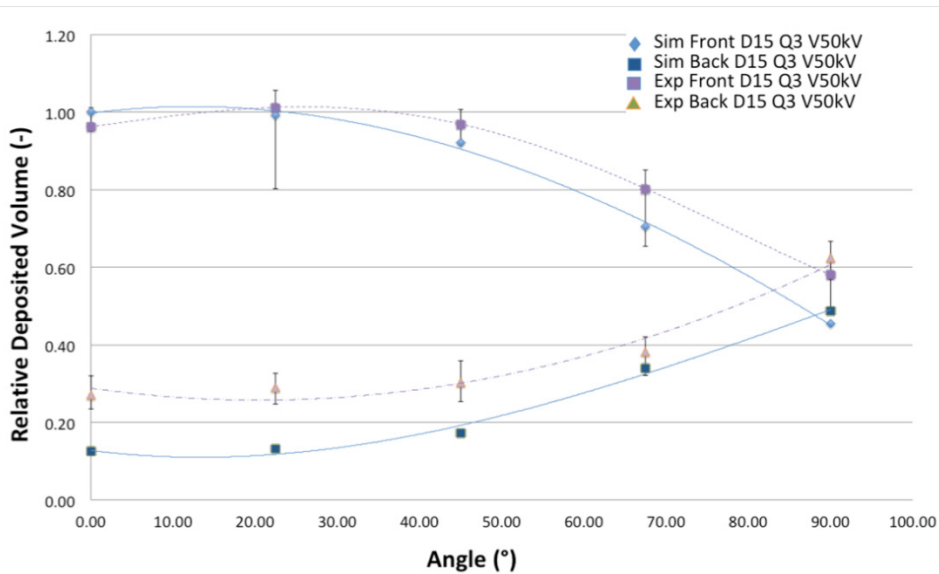


Fig.11: Quantitative comparison of relative deposited particle volume (normalized to maximum value) at front- and back-sides of 'small-plate' of simulations (blue, full) vs. processed measurement data (purple, dashed lines, including black bars for data variation limits) for varying the pistol angle to substrate at $Q=3\text{m}^3/\text{h}$, $U_{\text{eff}} = 50\text{kV}$ and $D=15\text{cm}$. Each depicted measurement data point is the median of three independent experiments and three consecutive thickness measurements per experiment.

3. DISCUSSIONS

A Eulerian-Lagrangian OpenFOAM® model was evolved from a rudimentary flow-particle solver under OpenFOAM® 1.4.1 to a parallelizable OpenFOAM® 5.0 module, capable of predicting the motion of deposition particles through a deposition pistol, past a high voltage electrode, across any deposition chamber, towards a grounded substrate and either onto the substrates' surface or towards an air vent. The results yield deposition patterns, which can be evaluated in order to predict the deposition quality in light of chosen process parameters and/or deposition pistol designs. Since the model works on the cloud computing software KaleidoSim®, which enables browser-based accessibility as well as the simultaneous running of hundreds of simulation cases, it can, as of now, be used to test large parameter windows of possible process settings. The latter capability thus constitutes the basis for optimizing deposition quality for any given substrate geometry.

The resulting deposition pattern predictions were studied by extensive experiments and simulated. Thereby, validating qualitatively and quantitatively deposition process parameters. Following key conclusions can be drawn from the study:

3.1. Relative deposited volume against applied voltage

According to Fig.8 qualitative simulated and measured 'relative deposited volume' trends against applied voltage U match quite well (both depicted trend curves are 3rd order polynomials). Both simulation and measurement show that increased U increases 'relative

deposited volume', where the effect is strong, as compared to the impact of other process parameters, but decreases at very high voltages. System parameter windows have been observed, which show a decrease in 'relative deposited volume' for increasing effective voltages beyond $U_{\text{eff}} > 50\text{kV}$. However, those are not discussed in this article. The maximum quantitative deviation between simulated and measured 'relative deposited volume' trends against U is $\Delta < 0.12$.

3.2. Relative deposited volume against airflow rate

According to Fig.9, the simulated 'relative deposited volume' trend against applied airflow rate Q shows negative curvature (depicted trend curve is a 3rd order polynomial) while the measured trend of median values can be approximated linearly. However, measurements feature large data variation limits in relation to the observed differences in curvature. Both simulation and measurement show that increased Q reduces the amount of 'relative deposited volume', where the effect is rather weak, as compared to the impact of other process parameters. The maximum quantitative deviation between simulated and measured 'relative deposited volume' trends is $\Delta < 0.07$.

3.3. Relative deposited volume against the distance between pistol and substrate

According to Fig.10, both simulated and measured 'relative deposited volume' trends against the distance between pistol and substrate D , for front- and back- sides can be approximated linearly (see trend curves) where qualitative trends match rather well. In addition, the measurements feature relatively small data variation limits. Both simulation and measurement show that increased D reduces the amount of relative deposited volume on the plate's front side strongly, while the deposition result on the back- side remains relatively unaffected, as compared to the impact of other process parameters. The maximum quantitative deviation between simulated and measured 'relative deposited volume' trends against D is $\Delta < 0.06$.

3.4. Relative deposited volume against angle between pistol and substrate

According Fig.11 simulated and measured 'relative deposited volume' trends against the angle between pistol and substrate at the front- and back- sides of the 'small-plate', matched quite well (both depicted trend curves are 3rd order polynomials). Both simulation and measurement show that increased angle reduces the amount of relative deposited volume on the plate's front side, while expectedly increasing it on the back side until an overlap occurs at 90° . The maximum quantitative deviation between simulated and measured 'relative deposited volume' trends against angle is $\Delta < 0.15$.

On this basis the model is currently and will in the near future be applied to develop i) deposition pistol nozzle designs, ii) innovative deposition process concepts, and iii) deposition chamber assemblies.

REFERENCES

- [1] Boiger, G. (2016) Characterization of particle-laden flows and deposition behaviour in electro-static fields. *Int. Journal of Multiphysics*. 10(2), pp. 195–204(10).
- [2] Boiger, G. (2016) Eulerian-LaGrangian model of particle laden flows and deposition effects in electro-static fields based on OpenFoam. *Int. Journal of Multiphysics*. 10(2), pp. 177–194(8).
- [3] Zubiaga, A., Brunner, D., Sager, F., Clemens, M., Koepf, E., Boiger, G. (2019) Faraday instability in small vessels under vertical vibration. *Int. Journal of Multiphysics*. 13(1), pp. 61-71.
- [4] Brunner, D., Boldrini, M., Boiger, G. (2017) Model based analysis of forced and natural convection effects in an electrochemical cell. *Int. Journal of Multiphysics*. 11(1), pp. 97-111.
- [5] Brunner, D., Khawaja, H., Moatamedi, M., Boiger, G. (2018) CFD modelling of pressure and shear rate in torsionally vibrating structures using ANSYS CFX and COMSOL multiphysics. *Int. Journal of Multiphysics*. 12(4), pp. 349-358.
- [6] Boiger, G. (2015) System dynamic modeling approach for resolving the thermo-chemistry of wood gasification. *Int. Journal of Multiphysics*. 9(2), pp. 137-155.
- [7] Boiger, G. (2014) A thermo fluid dynamic model of wood particle gasification and combustion processes. *Int. Journal of Multiphysics*. 8(2), pp. 203-230.
- [8] Khawaja, H. (2018) Study of Sound Waves in Fluidized Bed using CFD-DEM Simulations. *Particuology*. 38, pp. 126 - 133.
- [9] Khawaja H., (2011) CFD-DEM simulation of minimum fluidisation velocity in two phase medium. *The International Journal of Multiphysics*, 5 (2) (2011), pp. 89-100.
- [10] Khawaja, H., (2015a) CFD-DEM and experimental study of bubbling in a fluidized bed. *The Journal of Computational Multiphase Flows*, 7(4), pp. 227-240.
- [11] Khawaja, H., (2015b) Review of the phenomenon of fluidization and its numerical modelling techniques, *The International Journal of Multiphysics*, 9(4), pp. 397-408.
- [12] Khawaja H., Scott, S. (2011) CFD-DEM simulation of propagation of sound waves in fluid particles fluidised medium. *Int. Journal of Multiphysics*, 5(1), pp. 47-60.
- [13] Khawaja H., Scott S., Virk M., Moatamedi M. (2012) Quantitative analysis of accuracy of voidage computations in CFD-DEM simulations. *The Journal of Computational Multiphase Flows*, 4(2), pp. 183-192.
- [14] Eidesen, H., Khawaja, H. Jackson, S. (2018) Simulation of the HDPE Pyrolysis Process. *Int. Journal of Multiphysics*. 12(1), pp. 79 - 88.
- [15] Siyahhan, B., Boldrini, M., Hauri, S., Reinke, N., Boiger, G. (2018) Procedure for experimental data assessment for numerical solver validation in the context of model-based prediction of powder coating patterns. *Int. Journal of Multiphysics*. 12(4), pp. 373-392(20).
- [16] Boiger, G., Boldrini, M., Siyahhan, B. (2018) Enhancing the understanding of complex phenomena in powder coating, by applying Eulerian-Lagrangian simulation methodology. *Multiphysics 2018. 13th International Conference of Multiphysics, Krakow, Poland, 13-14 December. International Society of Multiphysics. ISSN (online) 2409-1669.*
- [17] Boiger, G. (2018) Eliminating anomalies of CFD model results of the powder coating process by refining aerodynamic flow-particle interaction and by introducing a dynamic particle charging model. *Scientific tracks & abstracts: day 1. 3rd International Conference on Fluid Dynamics & Aerodynamics, Berlin, Germany, 25-26 October. London: conferenceseries.com.*

- [18] Boiger, G., Reinke, N., Boldrini, M., Weilenmann, S., Studerus, P. (2017) Dynamic modeling of ionized oxygen distribution within powder coating pistols. Multiphysics 2017. 12th International Conference of Multiphysics, Beijing, China, 14-15 December. International Society of Multiphysics. ISSN (online) 2409-1669.
- [19] Boiger, G., Mataln, M., Brandstätter, W. (2010) Simulation of Particle Filtration Processes in Deformable Media, Part 3.1: Basic concepts and particle-fluid force implementation of a non-spherical dirt particle solver. Int. Journal of Multiphysics. 3(4), pp. 407-232(26).
- [20] Boiger, G., Mataln, M., Brandstätter, W. (2010) Simulation of Particle Filtration Processes in Deformable Media, Part 3.2: Interaction modelling and solver verification of a non-spherical dirt particle solver. Int. Journal of Multiphysics. 3(4), pp. 433-454(22).
- [21] Vallier, A. (2009) Tutorial icoLagrangianFoam/solidParticle. Chalmers University of Technology, Goteborg, Sweden. Peer reviewed tutorial, Hakan Nilsson, CFD with OpenSource Software; December 2009.
- [22] Drew, D. (2019) Kaleidosim Software, retrieved August 2019, from <http://kaleidosim.com>.
- [23] Bariska A., Reinke N., (2011) Berührungslose thermische Schichtprüfung, School of Engineering, Zurich University of Applied Sciences (ZHAW), Winterthur, Switzerland. Swiss Engineering STZ, 2011, 57.16.

